

Infrared spectroscopy and modeling of co-crystalline CO₂-C₂H₂ aerosol particles. II. The structure and shape of co-crystalline CO₂-C₂H₂ aerosol particles

Thomas C. Preston and Ruth Signorell

Citation: *The Journal of Chemical Physics* **136**, 094510 (2012); doi: 10.1063/1.3690064

View online: <http://dx.doi.org/10.1063/1.3690064>

View Table of Contents: <http://scitation.aip.org/content/aip/journal/jcp/136/9?ver=pdfcov>

Published by the [AIP Publishing](#)

Articles you may be interested in

[CO₂ and C₂H₂ in cold nanodroplets of oxygenated organic molecules and water](#)

J. Chem. Phys. **141**, 18C506 (2014); 10.1063/1.4895549

[Infrared spectroscopy and modeling of co-crystalline CO₂-C₂H₂ aerosol particles. I. The formation and decomposition of co-crystalline CO₂-C₂H₂ aerosol particles](#)

J. Chem. Phys. **136**, 094509 (2012); 10.1063/1.3690063

[Phase, shape, and architecture of S F 6 and S F 6 / C O 2 aerosol particles: Infrared spectra and modeling of vibrational excitons](#)

J. Chem. Phys. **128**, 184301 (2008); 10.1063/1.2913535

[Simulations of structure II H 2 and D 2 clathrates: Potentials incorporating quantum corrections](#)

J. Chem. Phys. **128**, 064506 (2008); 10.1063/1.2825618

[A density-functional theory investigation of 3-nitro-1,2,4-triazole-5-one dimers and crystal](#)

J. Chem. Phys. **121**, 12523 (2004); 10.1063/1.1812258

 **AIP** | APL Photonics

APL Photonics is pleased to announce
Benjamin Eggleton as its Editor-in-Chief



Infrared spectroscopy and modeling of co-crystalline $\text{CO}_2 \cdot \text{C}_2\text{H}_2$ aerosol particles. II. The structure and shape of co-crystalline $\text{CO}_2 \cdot \text{C}_2\text{H}_2$ aerosol particles

Thomas C. Preston and Ruth Signorell^{a)}

Department of Chemistry, University of British Columbia, 2036 Main Mall, Vancouver, British Columbia V6T 1Z1, Canada

(Received 28 September 2011; accepted 3 December 2011; published online 6 March 2012)

Infrared absorption spectra of co-crystalline $\text{CO}_2 \cdot \text{C}_2\text{H}_2$ aerosol particles were modeled using a combination of two methods. Density functional theory was used to model several bulk $\text{CO}_2 \cdot \text{C}_2\text{H}_2$ co-crystal structures and to calculate their lattice energies and frequency-dependent dielectric tensors. This was necessary as there currently exists no crystallographic or refractive index data on co-crystalline $\text{CO}_2 \cdot \text{C}_2\text{H}_2$ due to its metastability. The discrete dipole approximation was then used to calculate infrared absorption spectra of different model particles using the dielectric tensors calculated using density functional theory. Results from these simulations were compared to the experimental spectrum of co-crystalline $\text{CO}_2 \cdot \text{C}_2\text{H}_2$ aerosol particles. The aerosol particles after the decomposition of the co-crystalline phase were studied in Part I. © 2012 American Institute of Physics. [<http://dx.doi.org/10.1063/1.3690064>]

I. INTRODUCTION

It has previously been established that C_2H_2 and CO_2 can form a co-crystal with a 1:1 stoichiometry.¹⁻³ In that series of thin film experiments, this co-crystal was demonstrated to be metastable and decomposed into the solid phases of its pure components. We have recently studied the same system as aerosols (hereafter referred to Part I) and found a similar behaviour: co-crystalline $\text{CO}_2 \cdot \text{C}_2\text{H}_2$ particles initially form and decompose over time into particles with domains of pure C_2H_2 and pure CO_2 .⁴ In all of this work, it has been possible to monitor decomposition and formation due to the differences in the infrared (IR) bands of the three phases.

Our aim here is to understand the origin of the IR bands of co-crystalline $\text{CO}_2 \cdot \text{C}_2\text{H}_2$ aerosol particles. There are two principle points to consider: (i) How the type of crystal structure of $\text{CO}_2 \cdot \text{C}_2\text{H}_2$ affects the optical modes of the crystal, and (ii) how particle morphology influences the IR band shapes. The main difficulties are the lack of any crystallographic information and refractive index data for co-crystalline $\text{CO}_2 \cdot \text{C}_2\text{H}_2$. In the absence of experimentally measured indices of refraction, one must rely on a molecular model to calculate the IR absorption spectra for small particles. For that purpose, knowledge of the phase of the particles is essential. However, attempts to obtain crystallographic information on this substance have not been successful.⁵ This failure is almost certainly due to the metastability of the co-crystal. Despite this lack of information, there has been speculation on the nature of the phase. It was initially thought that C_2H_2 and CO_2 formed a 2:1 $\text{C}_2\text{H}_2:\text{CO}_2$ phase.¹ Additional experiments revised this ratio to 1:1 and the unit cell of the co-crystal was proposed to be face-centered cubic.² Aside from some hints obtained from IR spectra, the justification for this

structure was based on the fact that both C_2H_2 and CO_2 (i) can form cubic crystals (Pa3 symmetry), (ii) are similar in size, (iii) share the same set of symmetry operations, and (iv) possess electric quadrupole moments without possessing electric dipole moments.

Based on the observations that were mentioned it is reasonable to restrict our attention to unit cells with a 1:1 stoichiometry that are constructed by replacing molecules in either cubic CO_2 cells or cubic C_2H_2 cells. To find energetically favourable crystal structures for $\text{CO}_2 \cdot \text{C}_2\text{H}_2$, we have investigated such cells using density functional theory (DFT), as implemented with the ABINIT code.⁶⁻⁸ From optimized crystal structures, dielectric functions were calculated. These dielectric functions were then incorporated into a model of the $\text{CO}_2 \cdot \text{C}_2\text{H}_2$ aerosol particles in order to simulate IR spectra. This step was implemented using the discrete dipole approximation (DDA).⁹⁻¹¹ These simulated spectra were then compared to experimental spectra and the validity of modeled crystal structures were evaluated.

Throughout this study, we strongly rely on the previous work that has been performed on both pure CO_2 and pure C_2H_2 in their crystalline phases and pure CO_2 , pure C_2H_2 , and mixed $\text{CO}_2 \cdot \text{C}_2\text{H}_2$ in their gas phases. These systems have been extensively studied due to the simplicity of the molecules involved, their relevance to a broad range of fields and their importance as model systems. As was mentioned above, both C_2H_2 and CO_2 exhibit no permanent dipole moments yet possess quadrupole moments. Measurements put the values of these moments at 4.2×10^{-26} to 8.4×10^{-26} esu for C_2H_2 and -4.3×10^{-26} to -4.57×10^{-26} esu for CO_2 .¹² With pure CO_2 , quadrupole-quadrupole interactions can be used to explain the cubic structure of its crystalline phase as this arrangement is the lowest in energy for such moments.¹³ This is not true for C_2H_2 whose low temperature crystalline phase is orthorhombic. Therefore, higher

^{a)}Electronic mail: signorell@chem-ubc.ca. Fax: +1 604 822-2847.

order electric moments are needed to describe the electrostatic portion of the intermolecular potential of C_2H_2 .^{14–16} When these are included, the optimized geometry is based upon the donor-acceptor interaction between a C_2H_2 carbon-carbon triple-bond and a C_2H_2 hydrogen. This is clearly seen in the orthorhombic primitive unit cell which consists of two C_2H_2 molecules arranged in a T-shape.

These electrostatic interactions also largely define the molecular configurations seen in gas phase studies of the van der Waals dimers of CO_2-CO_2 , $C_2H_2-C_2H_2$, and $CO_2-C_2H_2$.^{17–25} The configuration of CO_2 dimers is slipped parallel^{17,18,25} while the configuration of C_2H_2 dimers is T-shaped.^{19–21,25} These configurations are both favorable quadrupole-quadrupole interactions and in either of the homodimers, the energy difference between the two states is small.²⁵ The $CO_2-C_2H_2$ heterodimer has a structure which is completely predicted by electrostatics—both molecules are parallel with their centers of mass being joined by a perpendicular line.^{22–25} All of these examples illustrate that it should be possible to qualitatively understand the results of $CO_2 \cdot C_2H_2$ optimized cells in terms of electrostatics with an emphasis on quadrupole-quadrupole interactions. The importance of electrostatics in this co-crystal means that the semilocal DFT functional used here should be appropriate for describing structural effects and IR spectra.⁶ However, this functional does not capture dispersion interactions so that calculated lattice energies are not expected to be accurate.²⁶

II. EXPERIMENTAL

The experimental conditions used for the formation of the $CO_2 \cdot C_2H_2$ aerosols were described in detail in Part I. The IR spectra shown here were measured immediately after the injection of the gases into the bath gas cooling cell. The mole fraction of CO_2 in the aerosol particles is 0.35. As was discussed in Part I, for this fraction, nearly all of the CO_2 is found in the co-crystalline phase. This greatly simplifies analysis of these bands.

III. COMPUTATIONAL METHODS

The procedure used to calculate the IR absorption spectra of particles is described in detail below but can be summarized as follows: the bulk crystal structure of the substance of interest is optimized using ABINIT. With this optimized structure a dielectric tensor is then calculated. This tensor is then incorporated into a model of the shape of the $CO_2 \cdot C_2H_2$ aerosol particles and, using a discretization method (in our case DDA), the absorption cross-section of the particle is calculated.

A. ABINIT

Solid-state DFT calculations were performed with the ABINIT software package^{6–8} using Troullier-Martins pseudopotentials,²⁷ the Perdew-Burke-Ernzerhof parameterization of the exchange-correlation functional²⁸ within the generalized gradient approximation (GGA), and a kinetic energy cutoff for planewaves of 70 Ha. Crystal structures were

relaxed using Broyden-Fletcher-Goldfarb-Shanno (BFGS) minimization.²⁹

As implemented with ABINIT, dynamical matrices, high-frequency dielectric tensors, and Born effective charges were calculated using optimized unit cells.³⁰ From these values frequency-dependent dielectric tensors were constructed and diagonalized. The form of the dielectric tensors are³⁰

$$\epsilon_{\alpha\beta}(\omega) = \epsilon_{\alpha\beta}^{\infty} + \frac{4\pi}{\Omega_0} \sum_m \frac{S_{m,\alpha\beta}}{\omega_{T_m}^2 - \omega^2 + i\omega\gamma_m}, \quad (1)$$

where ω_{T_m} is the transverse optical (TO) mode, $\epsilon_{\alpha\beta}^{\infty}$ is the high-frequency dielectric constant, Ω_0 is the unit cell volume, $S_{m,\alpha\beta}$ is the mode-oscillator strength, and γ_m is the damping constant for the optical mode m . For a diagonal dielectric tensor, the real longitudinal optical (LO) modes of the lattice will be the roots of Eq. (1).³¹

B. DDA

Absorption spectra for particles were calculated using DDA as implemented with the DDSCAT code.¹¹ This method is described in detail in Ref. 9. Particles modeled here were constructed using an inter-dipole separation, d , of 0.2 nm. This spacing was chosen so that all particles satisfy the validity criterion for DDA.¹⁰ These are (i) the number of dipoles chosen is sufficient to accurately represent the shape of the particle chosen and (ii) the condition $2\pi d|m|/\lambda < 1$, where m is the complex index of refraction and λ is the wavelength of light, is always true. The dimensions of any particle modeled here are much smaller than the wavelength of light impinging on them (e.g., if a particle with a cubic shape was modeled the length of its sides would be less than 100 nm).

IV. RESULTS AND DISCUSSION

A. The optical modes of orthorhombic C_2H_2 and cubic CO_2

Prior to considering $CO_2 \cdot C_2H_2$ co-crystals, we first examined the applicability of solid-state DFT to molecular crystals composed of either pure CO_2 or pure C_2H_2 . The phases chosen for these crystals corresponded to those found in aerosol particles of the respective pure substances (when prepared under similar conditions to the $CO_2 \cdot C_2H_2$ particles discussed here). The phases are cubic (CO_2) and orthorhombic (C_2H_2).^{32,33}

Unlike the metastable $CO_2 \cdot C_2H_2$ co-crystal, there exists crystallographic and refractive index data for both cubic CO_2 (Ref. 32 and 34–37) and orthorhombic C_2H_2 .^{33,38} Cubic CO_2 has been extensively studied and several thin film experiments have extracted refractive index data in the mid-IR. In Table I, we have listed LO and TO modes for the two IR active fundamental modes of CO_2 —the ν_2 bend and the ν_3 anti-symmetric stretch. These were taken from the most recent of the studies listed above.³⁴

Crystalline C_2H_2 has two phases (orthorhombic and cubic) that have been characterized using x-ray^{39,40} and neutron³³ diffraction. These phases have also been studied using IR (Ref. 38 and 41–45) and Raman⁴⁵ spectroscopy. Despite this breadth of work, only Khanna *et al.*³⁸ have presented

TABLE I. Experimental and calculated longitudinal optical and transverse optical modes (cm⁻¹) and high-frequency dielectric constants for crystalline C₂H₂ and CO₂. Experimental and calculated modes (cm⁻¹) for gas phase C₂H₂ and CO₂. For the calculated crystalline modes, values without brackets are harmonic while values inside of brackets are corrected. See Sec. IV A for details on the procedure used to calculate this correction. For orthorhombic C₂H₂, all optical modes within a band are orthogonal. The high-frequency dielectric constant for CO₂ does not contain any subscripts as $\epsilon_{11}^{\infty} = \epsilon_{22}^{\infty} = \epsilon_{33}^{\infty}$.

	C ₂ H ₂ gas phase		C ₂ H ₂ orthorhombic phase		CO ₂ gas phase		CO ₂ cubic phase				
	Expt. ⁵⁶	Calc.	Expt. ³⁸	Calc.	Expt. ⁵⁶	Calc.	Expt. ³⁴	Calc.			
ν_3	3289	3344.7	ω_{T_1}	3223.1	3273.1 (3217.4)	ν_2	667	650.9	ω_T	654.8	643.4 (659.4)
			ω_{L_1}	3228.1	3287.4 (3231.6)				ω_L	660.0	645.0 (661.0)
			ω_{T_2}	3223.1	3273.3 (3217.5)				ω_T	661.0	647.1 (663.2)
			ω_{L_2}	3228.1	3287.5 (3231.8)				ω_L	670.5	657.9 (674.0)
ν_5	730	736.5	ω_{T_1}	745.4	791.6 (785.1)	ν_3	2349	2344.3	ω_T	2345.0	2345.2 (2349.9)
			ω_{L_1}	753.4	806.7 (800.1)				ω_L	2377.0	2373.9 (2378.6)
			ω_{T_2}	756.2	766.1 (759.5)				ϵ^{∞}	1.54	1.73
			ω_{L_2}	787.8	802.6 (796.0)						
			ω_{T_3}	769.2	793.5 (787.0)						
			ω_{L_3}	777.0	807.4 (800.9)						
			ϵ_{11}^{∞}	1.96	1.98						
			ϵ_{22}^{∞}	1.96	1.98						
			ϵ_{33}^{∞}	1.96	1.69						

refractive index data for orthorhombic C₂H₂ (no refractive index data exists for cubic C₂H₂ in the mid-IR). C₂H₂ has two IR active fundamental modes and in the orthorhombic phase, the ν_5 bending vibration gives rise to three optical modes (all orthogonal) and the ν_3 antisymmetric stretching vibration gives rise to two optical modes (both orthogonal).

The experimental wavenumbers of the optical modes of the solids listed in Table I were determined by fitting refractive index data from the referenced thin film experiments. In this fitting process each optical mode was modeled with a single Lorentzian oscillator (e.g., the ν_2 band of CO₂ was fitted with two oscillators). For CO₂, this process was straightforward as its cubic crystal structure leads to an isotropic dielectric tensor ($\epsilon_{11} = \epsilon_{22} = \epsilon_{33}$). This is not the case for orthorhombic C₂H₂ which is a biaxial crystal ($\epsilon_{11} \neq \epsilon_{22} \neq \epsilon_{33}$). Furthermore, the thin film measurements of Khanna *et al.* were performed on polycrystalline samples. Therefore, it was necessary to use a directionally averaged index of refraction when fitting that data.⁴⁶ Additionally, we have listed the high-frequency dielectric constants for cubic CO₂ and orthorhombic C₂H₂ in Table I so that the summarized data can readily be used to construct dielectric functions with damping constants being added in an *ad hoc* manner, as is typical.⁴⁷

The parameters for the dielectric function of cubic CO₂ and orthorhombic C₂H₂ were calculated using the known crystallographic coordinates (after the structure was relaxed with ABINIT).^{32,33} Except for the optical modes associated with the C₂H₂ ν_5 band, the error between the calculated and observed frequencies was always less than 3%. As all of the ABINIT calculated frequencies are harmonic, correction terms were determined by taking the difference between the observed and calculated gas phase frequencies. This difference was then used to correct the calculated crystal frequencies. After this correction the error between the calculated and observed crystalline modes was lowered to less than 1%. This meant that the C₂H₂ ν_3 , the CO₂ ν_2 , and the CO₂ ν_3 bands

would be able to satisfactorily reproduce both position and shape in the modeled IR spectra of particles. The larger error in C₂H₂ ν_5 modes (up to 5.8%, even after the correction) meant that any dielectric function constructed using the calculated frequencies may not satisfactorily reproduce the band shape, although the band position will be within the listed errors. This discrepancy likely originates from the fact that the prepared C₂H₂ samples are not perfectly orthorhombic and contain a significant amount of disorder (see Ref. 48 for a discussion of this problem). This effect is more noticeable in the C₂H₂ ν_5 band than the C₂H₂ ν_3 band due to the larger transition dipole moment of ν_5 vibration. Therefore, it appears that, after correction, the optical modes associated with all but the C₂H₂ ν_5 band should be reliable in gauging the validity of a modeled crystal structure against measured IR spectra. In Sec. IV C, the correction terms determined here are also used to correct the calculated modes for the various CO₂ · C₂H₂ co-crystals.

B. Structure of CO₂ · C₂H₂ co-crystal

Currently, there exists no crystallographic information on the CO₂ · C₂H₂ co-crystal. Knowledge of this phase is, of course, essential when modeling the optical properties of particles using a microscopic model. As Part I shows clear evidence that a co-crystalline phase is formed under the present experimental conditions, possible crystal structures were investigated using ABINIT and the proposed 1:1 mixing ratio of C₂H₂:CO₂.²

For the starting structure, half of the C₂H₂ molecules in a cubic C₂H₂ cell were replaced with CO₂ molecules (Fig. 1(a), α -P2₁/c). This structure was chosen as both CO₂ and C₂H₂ form cubic crystal structures.^{32,33} Both the position of the center of mass and the alignment of the principle axes of the CO₂ molecules were identical to the C₂H₂ molecules that they replaced in the unit cell. Six different cells can be prepared using this procedure. However, all are equivalent so choosing

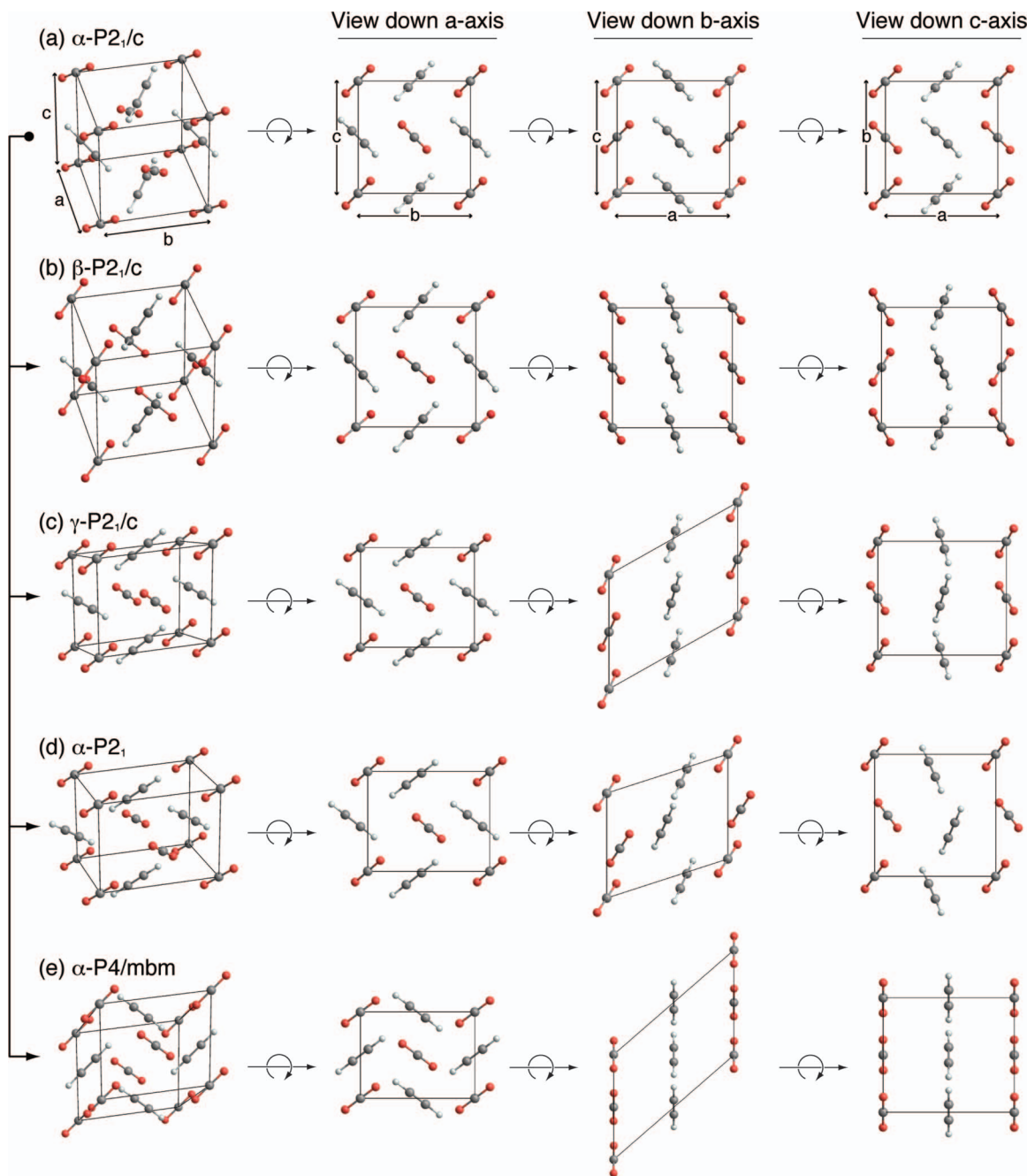


FIG. 1. $\text{CO}_2 \cdot \text{C}_2\text{H}_2$ co-crystals that are formed when cell (a) is relaxed. The details and restrictions used in the various optimization procedures are discussed in Sec. IV B. After this process, the unit cells were rebuilt using the highest possible symmetry. These cells are shown in Fig. 2.

which C_2H_2 molecules are replaced is unimportant and only one unit cell needs to be considered. Additionally, it was found that replacing half the CO_2 molecules in a cubic CO_2 cell with C_2H_2 molecules gave equivalent final structures to the C_2H_2 cubic cell starting point. The C_2H_2 and CO_2 lattice parameters for the starting structures were taken from the literature.^{32,33}

The results of all the optimizations are summarized in Table II and the final unit cells are depicted in Fig. 2. The lattice energy, E_{lattice} , was calculated using the relation

$$-E_{\text{lattice}} = \frac{1}{N} \left(E_{\text{crystal}} - \sum_{j=1}^N E_j \right), \quad (2)$$

where N is the total number of molecules in the unit cell, and E_{crystal} and E_j are the static total DFT energy at $T = 0$ K for the molecules in the unit cell and the free molecule j , respectively. The calculated energies and cell parameters for cubic CO_2 , cubic C_2H_2 , and orthorhombic C_2H_2 are also listed in Table II. Experimental values for the lattice energies of the pure substances are typically two- to three-times greater than the values listed in Table II.^{14,16,49} This discrepancy was expected as it is well-known that GGA functionals provide a poor description of van der Waals interactions.^{6,26} Despite this deviation, these functionals *do* provide a very good description of vibrational properties,⁶ our primary interest in this work.

TABLE II. Cell parameters and lattice energies calculated using density functional theory within the generalized gradient approximation. See text for details on how the CO₂ · C₂H₂ cells were obtained. Illustrations of the CO₂ · C₂H₂ unit cells are shown in Fig. 2.

Phase	Lattice energy (kJ/mol)	Space group	Lattice parameters (Å)			Cell angles (°)			Cell volume (Å ³)
			<i>a</i>	<i>b</i>	<i>c</i>	α	β	γ	
Orthorhombic C ₂ H ₂	13.3835	<i>Cmca</i>	6.8138	6.1743	6.2192	90	90	90	261.65
Cubic C ₂ H ₂	12.0100	<i>Pa3</i>	6.3543	6.3543	6.3543	90	90	90	256.57
Cubic CO ₂	9.9677	<i>Pa3</i>	6.0457	6.0457	6.0457	90	90	90	220.97
β - <i>P2₁/c</i> CO ₂ · C ₂ H ₂	8.2271	<i>P2₁/c</i>	6.5098	6.5098	6.5098	90	90	90	275.87
γ - <i>P2₁/c</i> CO ₂ · C ₂ H ₂	10.8429	<i>P2₁/c</i>	7.3479	6.1736	6.1987	90	108	90	267.33
α - <i>P2₁</i> CO ₂ · C ₂ H ₂	10.9326	<i>P2₁</i>	6.9066	6.6240	5.6905	90	108	90	247.59
α - <i>P4/mbm</i> CO ₂ · C ₂ H ₂	10.9695	<i>P4/mbm</i>	6.2077	6.2077	7.1157	90	90	90	274.20

In the first optimization (Fig. 1(b), β -*P2₁/c*), lattice parameters could only change under the restriction that they remained equal ($a = b = c$). Cell angles were simply held constant ($\alpha = \beta = \gamma = 90^\circ$). The purpose of this restricted optimization was to ensure that the originally proposed 1:1 C₂H₂:CO₂ face-centered cubic cell² was maintained. In the second optimization (Fig. 1(c), γ -*P2₁/c*), no restrictions were placed on the cell. This unit cell remains in the same space group as both α -*P2₁/c* and β -*P2₁/c*, however the lattice constants are now all unequal and one of the cell angles is no longer equal to 90° . This unit cell is obviously no longer face-centered cubic.

In both β -*P2₁/c* and γ -*P2₁/c*, C₂H₂ is located on sites with *C_i* symmetry. Therefore, we anticipate that the ν_2 mode of C₂H₂ (the symmetric stretch) will not be IR active. This means that these cells alone cannot explain the actual CO₂ · C₂H₂ cell as this band is experimentally observed to be IR active (see Sec. IV C). To address this issue, cells with different symmetries were examined by “breaking” the symmetry of either α -, β -, or γ -*P2₁/c* and relaxing the cells for

a second time. This was done by either displacing molecules from their equilibrium positions or by changing the primitive cell vectors. The amount of change introduced with either of these methods was typically small. Also note that this procedure was by no means comprehensive. Of all the structures that were obtained during this process only two had higher lattice energies than γ -*P2₁/c*. These were α -*P2₁* and α -*P4/mbm*. The unit cell of α -*P2₁* was the lowest in symmetry (monoclinic, *P2₁*) and C₂H₂ is now located on sites with *C₁* symmetry. Consequently, the C₂H₂ ν_2 mode is IR active. The unit cell of α -*P4/mbm* actually had a higher symmetry (tetragonal, *P4/mbm*) than the other cells studied here. While its C₂H₂ ν_2 mode is not IR active, this co-crystal is included here as it had a similar lattice energy as γ -*P2₁/c* and α -*P2₁* (it is slightly higher).

An analysis of the arrangement of the molecules in these unit cells is essential for identifying which intermolecular interactions are primarily responsible for changes in bond force constants. This will aid in understanding the shifts in modes that occur between the pure and mixed crystal phases as it will help identify the key interactions that are likely present in the true CO₂ · C₂H₂ cell. For simplicity, we will focus on the simple electrostatic interactions discussed in the Introduction for homo- and hetero-dimers of C₂H₂ and CO₂.

The quadrupole moments of C₂H₂ and CO₂ are opposite in sign, so the chosen starting structure α -*P2₁/c*, which is optimal for the case of all molecules having moments of the same sign, should not be at an energy minimum. Indeed, during all of the optimizations, molecules rotate out of their initial alignments and attempt to form alternating sheets of pure C₂H₂ and pure CO₂. These sheets are constructed as pairs of molecules attempt to form the energetically favorable T-shape, homodimer configuration. When no restrictions are in place (γ -*P2₁/c*, α -*P2₁*, α -*P4/mbm*) these sheets also slide against each other as C₂H₂ and CO₂ from adjacent sheets attempt to form the energetically favorable parallel heterodimer.

The result of these dilational and rotational motions are clearly seen in Fig. 1. When viewed down their *b*-axes in Fig. 1, the angle between the *a* and *c* axes has substantially changed from 90° for γ -*P2₁/c*, α -*P2₁*, and α -*P4/mbm*. The molecules in these cells have all rotated towards the plane defined by *b* and *c* axes. If the formation of T-shape homodimers and parallel heterodimers truly is driving the transformation of the cells forward, then cell α -*P4/mbm* represents the

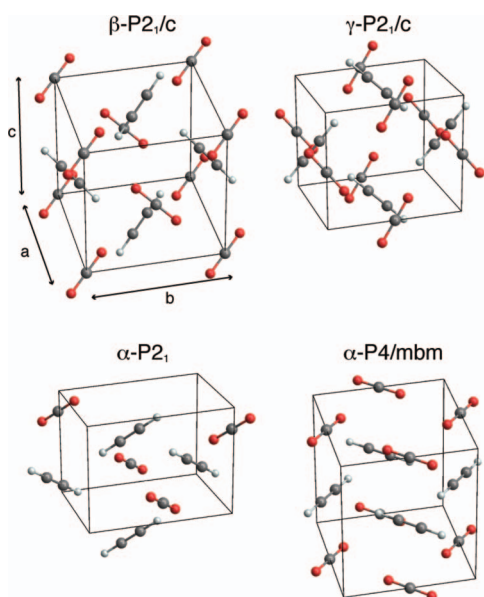


FIG. 2. CO₂ · C₂H₂ unit cells obtained by relaxing the cell shown in Fig. 1(a). Unlike the corresponding cells in Figs. 1(b)–1(e), these unit cells satisfy the symmetry requirements and cell parameters listed in Table II.

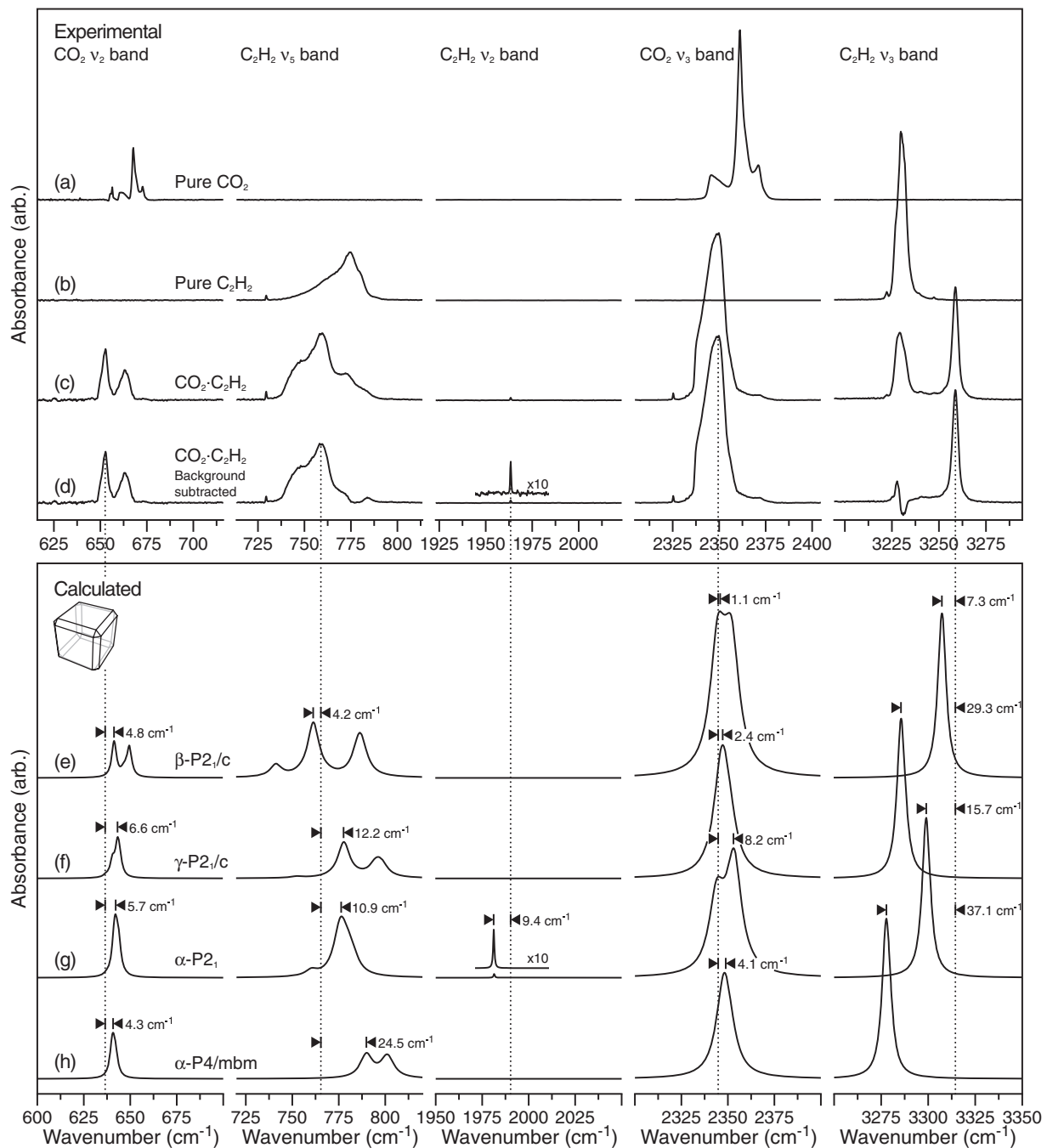


FIG. 3. Experimental infrared spectra for aerosol particles composed of (a) pure CO₂, (b) pure C₂H₂, (c) CO₂·C₂H₂, and (d) CO₂·C₂H₂ where bands associated with pure C₂H₂ have been subtracted. Infrared spectra calculated using a truncated cube particle model (see inset) and the dielectric functions generated using (e) β -P2₁/c, (f) γ -P2₁/c, (g) α -P2₁, and (h) α -P4/mbm. For each optical mode damping was set to a percentage of the ω_T of that mode. These were: 0.45%, 0.40%, 1.00%, 0.15%, and 0.04% for the CO₂ ν_2 , CO₂ ν_3 , C₂H₂ ν_5 , C₂H₂ ν_3 , and C₂H₂ ν_2 bands, respectively.

completion of this process. The molecules in this unit cell are in both of these arrangements with little distortion. This co-crystal also has a higher lattice energy than β -P2₁/c, γ -P2₁/c, or α -P2₁. In contrast, for the molecules in γ -P2₁/c and α -P2₁ this motion appears to become hindered during the transformational process as the arrangement of molecules into the T-shape homodimers and parallel heterodimers is not optimal. From the IR response calculated below it becomes clear that the amount of distortion has a large influence on the positions of the modes.

C. Analysis of IR spectra and optical modes of CO₂·C₂H₂

Due to the absence of index of refraction measurements from the previous CO₂·C₂H₂ thin film studies, a direct comparison between calculated and experimental dielectric functions was not possible. Instead, the validity of the CO₂·C₂H₂ unit cells discussed above was evaluated through (i) a comparison of the calculated and experimental spectra of particles (Fig. 3) and (ii) a comparison of the calculated and experimental TO modes (Table III). The experimental TO modes

TABLE III. Experimental and calculated transverse optical modes (cm⁻¹) for CO₂ · C₂H₂ co-crystals (see Fig. 2 for unit cells). Modes in brackets have been corrected (see Sec. IV A). Italicized modes are not infrared active. The experimental ν₃ ¹²CO₂ mode, which was not reported in Ref. 1–3, was determined from the position of the ¹³CO₂ mode in CO₂ · C₂H₂ and the observed isotopic frequency ratio between the ν₃ modes in ¹³CO₂ and ¹²CO₂ in crystalline CO₂. % Error is equal to (|Calc. – Expt. / Expt.) × 100%.

	Expt. ¹⁻³	<i>β</i> -P2 ₁ / <i>c</i>		<i>γ</i> -P2 ₁ / <i>c</i>		<i>α</i> -P2 ₁		<i>α</i> -P4/ <i>mbm</i>	
		Calc.	% Error	Calc.	% Error	Calc.	% Error	Calc.	% Error
C ₂ H ₂ ν ₂	1964	1983.9 (1957.0)	1.01 (0.36)	1977.7 (1950.8)	0.70 (0.67)	1981.4 (1954.5)	0.89 (0.48)	1974.8 (1947.9)	0.55 (0.82)
		1990.8 (1963.9)	1.36 (0.00)	1987.9 (1961.0)	1.22 (0.15)	1988.5 (1961.6)	1.25 (0.12)	1986.4 (1959.5)	1.14 (0.23)
C ₂ H ₂ ν ₃	3256	3305.4 (3249.7)	1.52 (0.19)	3282.6 (3226.9)	0.82 (0.89)	3296.2 (3240.5)	1.23 (0.48)	3274.3 (3218.6)	0.56 (1.15)
		3305.6 (3249.9)	1.52 (0.19)	3282.8 (3227.1)	0.82 (0.89)	3296.5 (3240.8)	1.24 (0.47)	3274.3 (3218.6)	0.56 (1.15)
C ₂ H ₂ ν ₅	740	739.4 (732.9)	0.08 (0.97)	752.4 (745.8)	1.67 (0.79)	758.8 (752.3)	2.54 (1.66)	757.9 (751.4)	2.42 (1.54)
		753.2 (746.6)	1.78 (0.89)	769.4 (762.9)	3.97 (3.09)	767.3 (760.8)	3.70 (2.81)	783.8 (777.3)	5.92 (5.04)
		752	782.9 (776.4)	4.11 (3.24)	792.1 (785.6)	5.34 (4.47)	773.5 (766.9)	2.86 (1.99)	798.0 (791.5)
CO ₂ ν ₂	649	783.4 (776.9)	4.18 (3.31)	794.7 (788.1)	5.68 (4.81)	777.4 (770.9)	3.38 (2.51)	798.0 (791.5)	6.12 (5.25)
		640.0 (656.1)	1.39 (1.09)	636.8 (652.9)	1.88 (0.60)	637.0 (653.1)	1.84 (0.63)	636.3 (652.3)	1.96 (0.51)
		640.3 (656.4)	1.34 (1.14)	637.7 (653.7)	1.75 (0.73)	638.4 (654.5)	1.63 (0.85)	637.6 (653.7)	1.75 (0.73)
CO ₂ ν ₃	2340	646.0 (662.1)	1.82 (0.62)	642.3 (658.4)	2.39 (0.05)	639.9 (656.0)	2.75 (0.30)	640.1 (656.2)	2.72 (0.27)
		647.4 (663.4)	1.62 (0.83)	642.6 (658.7)	2.34 (0.11)	640.0 (656.1)	2.74 (0.29)	640.1 (656.2)	2.72 (0.27)
		2337.4 (2342.0)	0.11 (0.09)	2336.9 (2341.6)	0.13 (0.07)	2338.1 (2342.7)	0.08 (0.12)	2342.1 (2346.8)	0.09 (0.29)
		2342.7 (2347.4)	0.12 (0.32)	2343.9 (2348.6)	0.17 (0.37)	2342.0 (2346.7)	0.09 (0.29)	2342.1 (2346.8)	0.09 (0.29)
Mean % Error			1.57 (0.95)		2.06 (1.26)		1.87 (0.93)		2.34 (1.63)

used in Table III were taken from the thin film measurements of Gough *et al.*¹⁻³ For the calculated spectra in Figs. 3(e)–3(h), dielectric functions were generated using the procedure outlined in Sec. III A. These functions were incorporated into a truncated cube particle model (see inset of Fig. 3 for a depiction of the particle shape). The experimental spectra of pure CO₂, pure C₂H₂, and CO₂ · C₂H₂ particles are shown in Figs. 3(a)–3(c), respectively. Due to the difficulty in preparing CO₂ · C₂H₂ particles without the presence of pure C₂H₂, pure C₂H₂ bands were subtracted from Fig. 3(c) using Fig. 3(b). The dip in the C₂H₂ ν₃ band in Fig. 3(d) indicates that this process was not ideal. Finally, the relative positions of the wavenumbers listed on the abscissa in the experimental and calculated spectra are such that the experimental and calculated gas phase modes coincide for each band. This positioning corrects the calculated wavenumbers in a manner identical to that used in Sec. IV A for the modes of pure crystalline CO₂ and C₂H₂ (i.e., the upper abscissa represents the corrected wavenumbers for the calculated bands while the lower abscissa represents the harmonic wavenumbers for the calculated bands).

Previous work on pure CO₂ and pure C₂H₂ particles has demonstrated that particle shape can be determined through the analysis of vibrational bands.⁵⁰⁻⁵⁴ Therefore, it should be possible to gain insight into CO₂ · C₂H₂ particle shape and simultaneously evaluate the validity of the dielectric functions that have been calculated here. However, for CO₂ · C₂H₂, such an approach is complicated by several factors. First, there is no transition with an LO-TO splitting as large as the ν₃ band of CO₂ in pure CO₂. This means that shape dependent features of the spectrum will be more compressed and difficult to interpret (within the electrostatic limit, shape dependent peaks will have maxima in the region bound by LO and TO modes).⁵⁵ Second, the low symmetry of the CO₂ · C₂H₂ unit cells results in an increased number of non-degenerate op-

tical modes in the co-crystals when compared to the cubic CO₂. This will further complicate analysis as each band will now contain a larger number of peaks. Third, the low symmetry of these co-crystal unit cells means that analyzing a wide array of particle shapes with these calculated dielectric functions will be an enormous task. This is because, in general, there is no clear way to orient the polarization axes of the dielectric tensor relative to the symmetry axes of any arbitrary particle. However, there are cases when this is not a concern. For instance, any spherical particle shape or any particle shape whose symmetry group is cubic (e.g., cube, truncated cube, octahedron, tetrahedron, etc.). In these situations, only one irreducible representation will possess a net electric dipole moment that is non-vanishing. Consequently, when calculating the absorption spectrum of a distribution of such particles with random alignments, the orientation of the polarization axes of the dielectric tensor relative to the symmetry axes of the particle is unimportant. Finally, with the previous work on CO₂ the growth of the particles over time and the resulting changes to the spectrum provided insight into particle morphology. With CO₂ · C₂H₂ decomposing into pure CO₂ and pure C₂H₂ over time this type of information is not present (Part I). Due to these factors, in Fig. 3 we do not attempt to model any further CO₂ · C₂H₂ particles beyond a truncated cube. The influence of further particle shapes is, however, considered briefly in Sec. IV D and Fig. 4.

For the C₂H₂ ν₃ band, the experimental difference in peak position between pure C₂H₂ (3230.2 cm⁻¹) and CO₂ · C₂H₂ (3258.7 cm⁻¹) is 28.5 cm⁻¹. This shift is the largest among the IR active fundamental modes of both C₂H₂ and CO₂. Furthermore, the small LO-TO splitting for the optical modes in this band (typically around 5 cm⁻¹) means that particle shape will have little effect on peak position. Therefore, the position and shape of this band is approximately

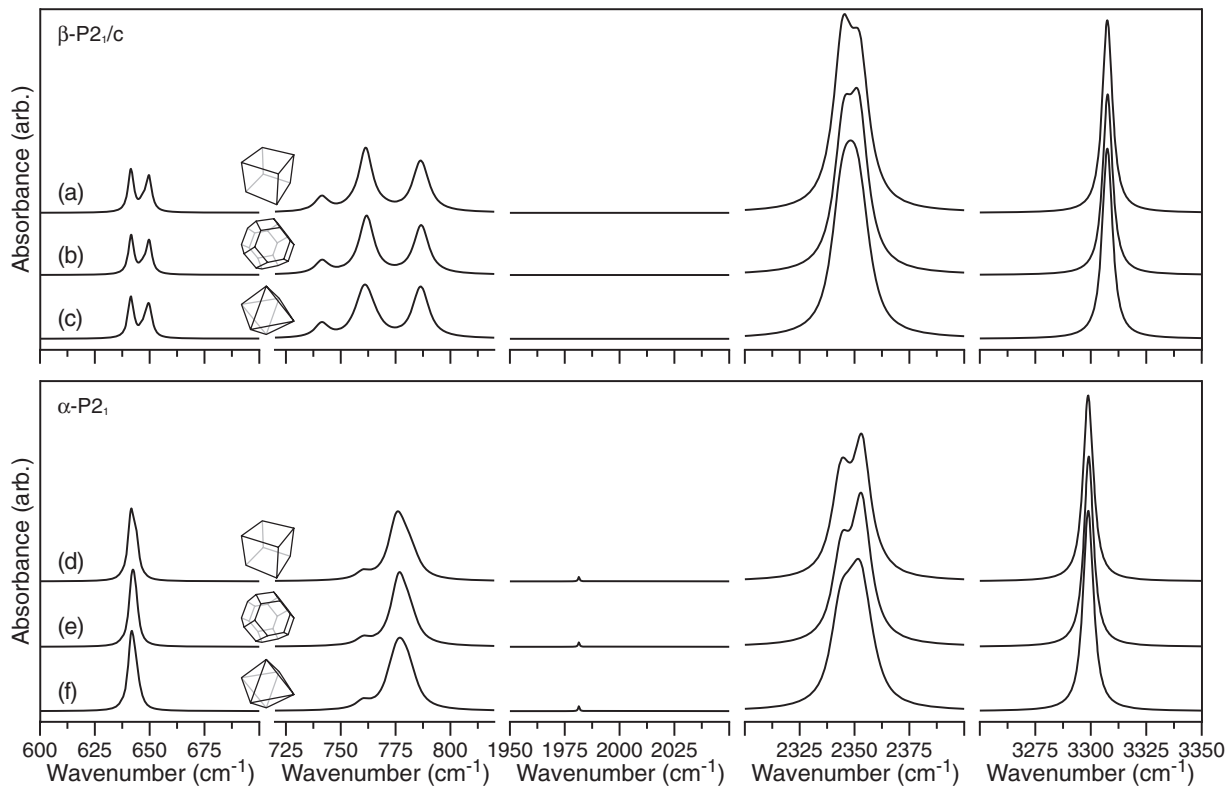


FIG. 4. Infrared spectra calculated using a cube (a and d), a truncated octahedron (b and e) and an octahedron (c and f). The dielectric functions used are those of β - $P2_1/c$ (a-c) and α - $P2_1$ (d-f). Damping constants for the optical modes are identical to those listed in the caption to Fig. 3.

independent of particle morphology and predominantly influenced by the configuration of the $\text{CO}_2 \cdot \text{C}_2\text{H}_2$ unit cell. Furthermore, the large difference in the position between pure C_2H_2 (Fig. 3(b)) and $\text{CO}_2 \cdot \text{C}_2\text{H}_2$ (Fig. 3(d)) for this band indicates its high sensitivity to the configuration of the unit cell and should therefore be an excellent probe of the unit cell structure.

Relative to the calculated C_2H_2 ν_3 TO modes in orthorhombic C_2H_2 (Table I), all of the calculated C_2H_2 ν_3 TO modes in the $\text{CO}_2 \cdot \text{C}_2\text{H}_2$ co-crystals are blue-shifted. This trend is consistent with what is experimentally observed. However, the magnitude of the predicted shift was found to vary significantly between co-crystals. The shifts for both γ - $P2_1/c$ and α - $P4/mbm$ are small, while for β - $P2_1/c$ and α - $P2_1$ they are much larger. Overall, in both Fig. 3 and Table III, we see that the IR response of the β - $P2_1/c$ co-crystal provides the best match to the experimental C_2H_2 ν_3 mode in the $\text{CO}_2 \cdot \text{C}_2\text{H}_2$ cell. Examination of the co-crystal cells in Fig. 1 and 2 reveals that the structural factor of primary influence on this shift is the configuration of the T-shape C_2H_2 - C_2H_2 interaction. The greater the disruption of this T-shape, the greater the shift. The interaction between the electronegative carbon-carbon triple bond and the electropositive hydrogen atom has a tremendous influence on the force constant of CH stretches. In the case of pure C_2H_2 , the orthorhombic cell is built in such a way that every hydrogen faces an electronegative carbon-carbon triple bond in a nearly optimal T-shape geometry (it is slightly distorted). All of the co-crystal configurations deviate in varying degrees from this configuration. The larger the deviation, the stronger the blue-

shift in the corresponding spectrum. Based on this analysis and the large experimental shift it seems likely that the true co-crystal contains C_2H_2 in a T-shape configuration that has been heavily distorted from the one in the orthorhombic unit cell of pure C_2H_2 .

A similar analysis should be possible for the CO_2 ν_3 band, where the oxygen-carbon force constant is reduced due to the intermolecular interaction between an electronegative oxygen with an electropositive oxygen. However, with a difference of only 11.5 cm^{-1} in the experimental band positions for pure CO_2 (2361.0 cm^{-1}) and $\text{CO}_2 \cdot \text{C}_2\text{H}_2$ (2349.5 cm^{-1}) and a much larger LO-TO splitting for the optical modes found in this band (relative to those found in the C_2H_2 ν_3 band) this type of analysis is not straightforward. In the calculated IR response for all of the $\text{CO}_2 \cdot \text{C}_2\text{H}_2$ co-crystals there is a small redshift in the CO_2 ν_3 TO modes relative to those found in cubic CO_2 . Table III shows that the error between the observed and calculated TO modes in this band is the smallest of the bands considered here. Examination of Fig. 3 reveals that it is very difficult to differentiate between the various $\text{CO}_2 \cdot \text{C}_2\text{H}_2$ unit cells based on this band. All of the changes due to unit cell configuration are simply far too minor.

A similar result is also found when analyzing the CO_2 ν_2 band shifts. The calculated IR response for the $\text{CO}_2 \cdot \text{C}_2\text{H}_2$ co-crystals differs only slightly from the calculated response for pure, cubic CO_2 . Relative to the calculated TO modes for cubic CO_2 , the TO modes of the co-crystal are all red-shifted (with the exception of one of the β - $P2_1/c$ modes). The calculated TO modes of the co-crystals are also all split. These

two trends are consistent with what is observed. The splitting between the ν_2 modes in this co-crystal is larger than any of the other structures and, when the spectrum of a β - $P2_1/c$ particle is calculated, two distinct peaks are observed in its CO₂ ν_2 band (Fig. 3(e)). This splitting is consistent with the experimental band (Fig. 3(d)) and is not observed in the other calculated CO₂ ν_2 bands (Figs. 3(f)–3(h)).

In Sec. IV A it was found that for orthorhombic C₂H₂ the amount of error in the calculated optical modes of the ν_5 vibration was much larger than any of the other IR active fundamental bands in either orthorhombic C₂H₂ or cubic CO₂. This meant that, when incorporated into a particle model, a dielectric function constructed using the optical modes of this band would not be able to satisfactorily reproduce experimental particle spectra. Therefore, basing any conclusion solely on this result is not advised. However, it is still worthwhile to make some statements on the calculated wavenumbers for this band. When the experimental spectra of pure C₂H₂ (Fig. 3(b)) and CO₂ · C₂H₂ (Fig. 3(d)) in this region are compared, there clearly must be a red-shift in the corresponding optical modes. This is found for the TO modes of β - $P2_1/c$, γ - $P2_1/c$, and α - $P2_1$ but not for those of α - $P4/mbm$, whose TO modes are all blue-shifted from those found in pure orthorhombic C₂H₂ (compare the calculated TO modes in Table I to those in Table III). Examining the C₂H₂ ν_5 band in the CO₂ · C₂H₂ spectra (Fig. 3), hints that the spectrum of the α - $P2_1$ particle provides the best agreement with the experimental band in terms of overall shape and position.

Finally, we consider the C₂H₂ ν_2 band, which is observed to be IR inactive in orthorhombic C₂H₂ but IR active in the CO₂ · C₂H₂ co-crystal. Clearly, the site symmetry of C₂H₂ in the actual co-crystal must allow for this mode to be IR active. Of all the modeled co-crystals, this only holds for α - $P2_1$. However, this does not mean the α - $P2_1$ is the correct co-crystal, only that perfect β - $P2_1/c$, γ - $P2_1/c$, and α - $P4/mbm$ are not. In fact, β - $P2_1/c$, γ - $P2_1/c$, and α - $P4/mbm$ may be closer to the actual structure of the co-crystal than α - $P2_1$. Simply moving one of the C₂H₂ molecules out of its symmetry site in any one of the unit cells in these co-crystals makes this band IR active without a large change to the overall unit cell structure. Therefore, the importance of this band in characterizing the crystal structure should not be overemphasized as it is sensitive to very small changes in crystal structure.

The results of this section can be summarized as follows: First, a 1:1 C₂H₂:CO₂ unit cell seems very likely. Any other stoichiometry would lead to large discrepancies between the calculated and observed CO₂ · C₂H₂ band intensities in Fig. 3, specifically to the ratio of the C₂H₂ to CO₂ intensities in the co-crystal spectra. Second, the C₂H₂-C₂H₂ configuration in the co-crystal unit cell is heavily distorted from the T-shape observed in orthorhombic C₂H₂. Therefore, despite its high lattice energy, a unit cell such as α - $P4/mbm$ is unlikely. Third, relative to how they are arranged in a cubic CO₂ unit cell, CO₂ molecules are moved towards a T-shape configuration in the co-crystal. However, comments on this change are not as definitive as those concerning the C₂H₂-C₂H₂ interaction as the observed and calculated frequency shifts are small. Fourth, as expected, only the α - $P2_1$ co-crystal yields an IR active C₂H₂ ν_2 band. However, many co-crystals with this

property were obtained during the symmetry breaking process (see Sec. IV B). Therefore, this property is not a definitive indicator of the correct unit cell. Overall, inspection of Fig. 3 in the region of the C₂H₂ ν_3 and ν_5 and the CO₂ ν_2 and ν_3 bands reveals that the IR spectrum of the β - $P2_1/c$ particle (Fig. 3(e)) provides the best correspondence to the experimental spectrum (Fig. 3(d)), while the α - $P4/mbm$ particle provides the poorest correspondence. The comparison of the experimental and calculated TO modes in Table III shows that the corrected TO modes of the α - $P2_1$ co-crystal have the lowest overall percent error. In summary, the β - $P2_1/c$ and α - $P2_1$ unit cells are the most promising candidates for the CO₂ · C₂H₂ unit cell. These two unit cells appear to correctly capture most the molecular configurations that exist in the actual co-crystal cell. In fact, since the energies of the unit cells are so similar, the CO₂ · C₂H₂ particles may contain contributions from multiple unit cells (many of which could contain imperfections).

D. Influence of shape on the IR spectra of CO₂ · C₂H₂ particles

We further explore the influence of particle shape on spectra by calculating the spectra for three further shapes with octahedral symmetry – a cube (Figs. 4(a) and 4(d)), a truncated octahedron (Figs. 4(b) and 4(e)) and an octahedron (Figs. 4(c) and 4(f)). As discussed in Sec. IV C, the orientation of the polarization axes within such particles is unimportant when considering a spectrum that has been averaged over all particle orientations. This greatly simplifies analysis. We only consider spectra generated using the dielectric function of the β - $P2_1/c$ and α - $P2_1$ phases as these gave the best overall correspondence to the observed spectrum and TO modes (see Sec. IV C).

Figure 4 reveals that there is little difference among the set of spectra belonging to the same crystal phase. This was expected for bands with small LO-TO splittings (the C₂H₂ ν_3 and ν_2 bands and the CO₂ ν_2 band). However, even the CO₂ ν_3 band, which has the largest LO-TO splitting, only shows a weak shape dependence when compared to particles composed of the pure CO₂. In pure cubic CO₂ the calculated LO-TO splitting is 28.7 cm⁻¹ while for β - $P2_1/c$ and α - $P2_1$ the largest LO-TO splittings in this band are 19.6 and 23.0 cm⁻¹, respectively. Similar comments apply to the C₂H₂ ν_5 band. For the pure orthorhombic crystal the largest calculated LO-TO splitting is 36.5 cm⁻¹ whereas for β - $P2_1/c$ and α - $P2_1$ the largest LO-TO splittings are 19.7 and 19.9 cm⁻¹, respectively. These results partially reflect the fact that in the co-crystal the densities of both C₂H₂ and CO₂ molecules are much lower than that of their respective pure crystalline forms. As a result of this lower density, transition-dipole coupling is reduced. This will lead to a decrease in LO-TO splitting and, consequently, shape effects will become less important.

The presence of non-degenerate optical modes in the CO₂ ν_3 band of the co-crystals further complicates spectra (relative to cubic CO₂). This effect has its origin in the low symmetry of the co-crystal unit cells. In general, it appears as if it is very difficult to comment on particle shape using the IR active bands of CO₂ · C₂H₂. Unlike particles of the pure substances,

the shape dependence is simply too weak and complicated to gain any insight. Furthermore, as discussed in detail in Sec. IV C, the low symmetry of the co-crystal unit cells makes the consideration of wide array of particles shapes an enormous task.

V. SUMMARY

IR spectroscopy reveals that co-condensation of CO₂ and C₂H₂ in a bath gas cooling cell initially leads to the formation of co-crystalline CO₂·C₂H₂ aerosol particles. The co-crystalline form is metastable and decomposes over time. As a consequence of this, its crystal structure is unknown. The present contribution uses DFT calculations (as implemented with ABINIT) to determine possible structures for these co-crystals as well as corresponding dielectric functions (in the mid-IR region). Aerosol IR spectra are calculated from these dielectric functions using DDA. Using several different crystal structures found with DFT, β -P2₁/c, and α -P2₁ (see Fig. 2 for unit cells) agree best with the experimental observations in the IR. Both of these cells have a 1:1 ratio of CO₂ to C₂H₂. As the energies of the unit cells are very similar, it is possible that several polymorphs crystallize when the aerosol particles form. A more detailed determination of the crystal structure(s) would require a thorough crystallographic study. However, this poses a serious challenge due to the metastability of the co-crystalline phase. Calculated IR spectra show little dependence on the particle shape, in contrast to what is observed for pure crystalline CO₂ and C₂H₂ particles. The lack of shape sensitivity has its origin in the low symmetry of the co-crystal unit cells and the smaller LO-TO splitting when compared to the pure crystalline CO₂ and C₂H₂.

ACKNOWLEDGMENTS

Financial support from the Natural Sciences and Engineering Research Council of Canada (NSERC) and the Canada Foundation for Innovation is gratefully acknowledged. This research has been enabled through the generous allocation of advanced computing resources by WestGrid and Compute/Calcul Canada. T.C.P. acknowledges a NSERC fellowship and R.S. acknowledges a NSERC E. W. R. Steacie memorial fellowship.

- ¹T. E. Gough and T. E. Rowat, *J. Chem. Phys.* **102**, 3932 (1995).
- ²T. E. Gough and T. E. Rowat, *J. Chem. Phys.* **109**, 6809 (1998).
- ³T. E. Gough, T. E. Rowat, and R. Illner, *Chem. Phys. Lett.* **298**, 196 (1998).
- ⁴T. C. Preston, C. C. Wang, and R. Signorell, *J. Chem. Phys.* **136**, 094509 (2012).
- ⁵M. T. Kirchner, D. Bläser, and R. Boese, *Chem.-Eur. J.* **16**, 2131 (2010).
- ⁶X. Gonze, J.-M. Beuken, R. Caracas, F. Detraux, M. Fuchs, G.-M. Rignanese, L. Sindic, M. Verstraete, G. Zerah, F. Jollet, M. Torrent, A. Roy, M. Mikami, Ph. Ghosez, J.-Y. Raty, and D. C. Allan, *Comput. Mater. Sci.* **25**, 478 (2002).
- ⁷X. Gonze, G.-M. Rignanese, M. Verstraete, J.-M. Beuken, Y. Pouillon, R. Caracas, F. Jollet, M. Torrent, G. Zerah, M. Mikami, Ph. Ghosez, M. Veithen, J.-Y. Raty, V. Olevano, F. Bruneval, L. Reining, R. Godby, G. Onida, D. R. Hamann, and D. C. Allan, *Z. Kristallogr.* **220**, 558 (2005).

- ⁸The ABINIT code is a common project of the Université Catholique de Louvain, Corning Incorporated, and other contributors, see <http://www.abinit.org>.
- ⁹B. T. Draine, *Astrophys. J.* **333**, 848 (1988).
- ¹⁰B. T. Draine and P. J. Flatau, *J. Opt. Soc. Am. A* **11**, 1491 (1994).
- ¹¹B. T. Draine and P. J. Flatau, e-print arXiv:0809.0337v5.
- ¹²C. G. Gray and K. E. Gubbins, *Theory of Molecular Fluids. Volume 1: Fundamentals* (Clarendon Press, Oxford, 1984).
- ¹³O. Nagai and T. Nakamura, *Prog. Theor. Phys.* **24**, 432 (1960).
- ¹⁴F. L. Hirshfeld and K. Mirsky, *Acta Cryst. A* **35**, 366 (1979).
- ¹⁵Z. Gamba and H. Bonadeo, *J. Chem. Phys.* **76**, 6215 (1982).
- ¹⁶M. Marchi and R. Righini, *Chem. Phys.* **94**, 465 (1985).
- ¹⁷K. W. Jucks, Z. S. Huang, D. Dayton, R. E. Miller, and W. J. Lafferty, *J. Chem. Phys.* **86**, 4341 (1987).
- ¹⁸K. W. Jucks, Z. S. Huang, R. E. Miller, G. T. Fraser, A. S. Pine, and W. J. Lafferty, *J. Chem. Phys.* **88**, 2185 (1988).
- ¹⁹D. G. Prichard, R. N. Nandi, and J. S. Muentner, *J. Chem. Phys.* **89**, 115 (1988).
- ²⁰Y. Ohshima, Y. Matsumoto, and M. Takami, *Chem. Phys. Lett.* **147**, 1 (1988).
- ²¹G. T. Fraser, R. D. Suenram, F. J. Lovas, A. S. Pine, J. T. Hougen, W. J. Lafferty, and J. S. Muentner, *J. Chem. Phys.* **89**, 6028 (1988).
- ²²D. G. Prichard, R. N. Nandi, J. S. Muentner, and B. J. Howard, *J. Chem. Phys.* **89**, 1245 (1988).
- ²³J. S. Muentner, *J. Chem. Phys.* **90**, 4048 (1989).
- ²⁴Z. S. Huang and R. E. Miller, *Chem. Phys.* **132**, 185 (1989).
- ²⁵R. G. A. Bone and N. C. Handy, *Theor. Chim. Acta* **78**, 133 (1990).
- ²⁶H. Liu, J. Zhao, D. Wei, and Z. Gong, *J. Chem. Phys.* **124**, 124501 (2006).
- ²⁷N. Troullier and J. L. Martins, *Phys. Rev. B* **43**, 1993 (1991).
- ²⁸J. P. Perdew, K. Burke, and M. Ernzerhof, *Phys. Rev. Lett.* **77**, 3865 (1996).
- ²⁹H. B. Schlegel, *J. Comput. Chem.* **3**, 214 (1982).
- ³⁰X. Gonze and C. Lee, *Phys. Rev. B* **55**, 10355 (1997).
- ³¹L. Merten and R. Clause, *Phys. Status Solidi B* **89**, 159 (1978).
- ³²R. W. G. Wyckoff, *Crystal Structures* (Wiley, New York, 1963).
- ³³R. K. McMullan, Å. Kvik, and P. Popelier, *Acta Crystallogr., Sect. B: Struct. Sci.* **48**, 726 (1992).
- ³⁴G. A. Baratta and M. E. Palumbo, *J. Opt. Soc. Am. A* **15**, 3076 (1998).
- ³⁵S. G. Warren, *Appl. Opt.* **25**, 2650 (1986).
- ³⁶D. M. Hudgins, S. A. Sandford, L. J. Allamandola, and A. G. G. M. Tielens, *Astrophys. J., Suppl. Ser.* **86**, 713 (1993).
- ³⁷P. Ehrenfreund, A. C. A. Boogert, P. A. Gerakines, A. G. G. M. Tielens, and E. F. Dishoeck, *Astron. Astrophys.* **328**, 649 (1997).
- ³⁸R. K. Khanna, M. J. Ospina, and G. Zhao, *Icarus* **73**, 527 (1988).
- ³⁹T. Sugawara and E. Kanda, *Sci. Rep. Res. Inst. Tôhoku Univ. A* **4**, 607 (1952).
- ⁴⁰G. J. H. van Nes and F. van Bolhuis, *Acta Crystallogr., Sect. B: Struct. Sci.* **35**, 2580 (1979).
- ⁴¹G. L. Bottger and D. F. Eggers, *J. Chem. Phys.* **40**, 2010 (1964).
- ⁴²D. A. Dows, *Spectrochim. Acta* **22**, 1479 (1966).
- ⁴³A. Anderson and W. H. Smith, *J. Chem. Phys.* **44**, 4216 (1966).
- ⁴⁴W. H. Smith, *Chem. Phys. Lett.* **3**, 464 (1969).
- ⁴⁵A. Anderson, B. Andrews, and B. H. Torrie, *J. Raman Spectrosc.* **16**, 202 (1985).
- ⁴⁶R. E. Newnham, *Properties of Materials: Anisotropy, Symmetry, Structure* (Oxford University Press, Toronto, 2005).
- ⁴⁷B. Donovan and J. F. Angress, *Lattice Vibrations* (Chapman and Hall, London, 1971).
- ⁴⁸T. C. Preston, G. Firanescu, and R. Signorell, *Phys. Chem. Chem. Phys.* **12**, 7924 (2010).
- ⁴⁹H. Spöner and M. Bruch-Willstätter, *J. Chem. Phys.* **5**, 745 (1937).
- ⁵⁰R. Disselkamp and G. E. Ewing, *J. Chem. Phys.* **99**, 2439 (1993).
- ⁵¹T. E. Gough and T. Wang, *J. Chem. Phys.* **105**, 4899 (1996).
- ⁵²R. Signorell and M. K. Kunzmann, *Chem. Phys. Lett.* **371**, 260 (2003).
- ⁵³Ó. F. Sigurbjörnsson, G. Firanescu, and R. Signorell, *Annu. Rev. Phys. Chem.* **60**, 127 (2009).
- ⁵⁴C. C. Wang, P. Zielke, Ó. F. Sigurbjörnsson, C. R. Viteri, and R. Signorell, *J. Phys. Chem. A* **113**, 11129 (2009).
- ⁵⁵C. F. Bohren and D. R. Huffman, *Absorption and Scattering of Light by Small Particles* (Wiley, New York, 1983).
- ⁵⁶D. R. Lide, *CRC Handbook of Chemistry and Physics*, 84th ed. (CRC, Boca Raton, FL, 2003).